Article:
Caro-León, FJ, Argüelles-Monal, W, Carvajal-Millán, E et al. (4 more authors) (2018) Production and characterization of supercritical CO_2 dried chitosan nanoparticles as novel carrier device. Carbohydrate Polymers, 198. pp. 556-562. ISSN 0144-8617

https://doi.org/10.1016/j.carbpol.2018.06.102

Production and characterization of supercritical CO_2 dried chitosan nanoparticles as novel carrier device

F. J. Caro-León,[a] J. Lizardi-Mendoza,[a*] W. Argüelles-Monal,[b] E. Carvajal-Millan,[a] Y. L. López-Franco,[a] F. Goycoolea-Valencia[c] and Julio San Román[d].

[a]Centro de Investigación en Alimentación y Desarrollo A.C., Grupo de Investigación en Biopolímeros. Carr. a La Victoria km 0.6, Hermosillo, Sonora, Mexico, 83304.

[b]Centro de Investigación en Alimentación y Desarrollo A.C.; Coord. Reg. Guaymas, Grupo de Investigación en Polímeros Naturales. Carr. a Varadero Nacional km. 6.6, Guaymas, Sonora, Mexico, 85480.

[c]School of Food Science and Nutrition,University of Leeds, Woodhouse Ln, Leeds, UK, LS2 9JT.

[d]Grupo de Investigación de Biomateriales, Departamento de Nanomateriales Poliméricos y Biomateriales, Instituto de Ciencia y Tecnología de Polímeros, CSIC, Juan de la Cierva, 3, Madrid, Spain, 28006.

*Corresponding author. E-mail: jalim@ciad.mx. 01-52-(662)2892400 ext 248.

E-mail addresses: Javier.caro@estudiantes.ciad.mx (F. J. Caro-León), jalim@ciad.mx (J. Lizardi-Mendoza), waldo@ciad.mx (W. Argüelles-Monal), ecarvajal@ciad.mx (E. Carvajal-Millan), lopezf@ciad.mx (Y. L. López-Franco), F.M.Goycoolea@leeds.ac.uk (F. Goycoolea-Valencia), jsroman@ictp.csic.es (J. San Román).

Abstract

Materials obtained by the supercritical CO_2 drying technology have outstanding structural properties that allow the incorporation of molecules in their porous structure. In this context, dried chitosan nanoparticles including β-lactoglobulin were obtained. The chitosan nanoparticles were produced by ionotropic gelation incorporating the protein followed by a solvent exchange and CO_2 supercritical drying procedure. The loading parameters demonstrate high incorporation efficiency that is preserved after the supercritical drying. The physicochemical characteristics and structural properties were determined corroborating the presence of the protein in the material. The release of the β-lactoglobulin was highly influenced by the pH, reaching around 40% at acidic conditions in 10 hours. The protein loaded supercritical CO_2 dried chitosan nanoparticles can be effectively resuspended in acidic aqueous medium displaying moderate antioxidant activity which indicate its potential application as a biomaterial and controlled release device in biological environments.

Abbreviations

Supercritical drying ($scCO_2D$); chitosan (Cs); sodium tripolyphosphate (TPP); β-Lactoglobulin (βlg); chitosan nanoparticles gel (CsN); chitosan nanoparticles with β-Lactoglobulin (CsNβ); dry chitosan nanoparticles (DCsN); dry chitosan nanoparticles gels with βlg (DCsNβ); solid-state cross-polarization magic angle spinning ^{13}C nuclear magnetic resonance (CP/MAS-NMR); attenuated total reflection Fourier transform infrared (ATR-FTIR); thermogravimetric analysis (TGA); differential scanning calorimetry (DSC); X-ray diffraction (XRD); Brunauer–Emmett–Teller (BET); 1, 1-Diphenyl-2-picrylhydrazyl (DPPH); (3-(4,5-Dimethylthiazol-2-yl)-2,5-Diphenyltetrazolium Bromide) (MTT).

Keywords: Chitosan; Nanoparticles; Dry gel; CO_2 Supercritical drying; Ionotropic gelation; β-lactoglobulin.

1. Introduction

The nanobiotechnology comprises the knowledge related with the production, characterization and application of nanomaterials in life sciences, including medicine (Fakruddin, Hossain, & Afroz, 2012). Some remarkable advances in the field are the development of biosensors, improved contrast agents for imaging and therapeutic compounds delivery devices. Particularly for the drug delivery technology there is a search for materials that provide improved controlled release features of the incorporated molecules enabling the reduction of dosages and undesirable side effects of therapeutic agents (Safari & Zarnegar, 2014). To this end, the use of synthetic or natural polymers (i.e. proteins or polysaccharides) provide the mechanical-structural features to generate a diversity of materials, such as nanocapsules, nanoparticles, nanomicelles, nanospheres or nanoporous materials (Carvalho, Grenha, Remuñán-López, Alonso, & Seijo, 2009; Cavalli, Leone, Minelli, Fantozzi, & Dianzani, 2014; Goimil et al., 2017; Larson & Ghandehari, 2012; Mohanraj, Barnes, & Prestidge, 2010; Yang et al., 2009).

Chitosan (Cs) is a polysaccharide composed of 2 acetamide 2 deoxy-D glucopyranose and 2 amino-2 deoxy-D glucopyranose units linked by β(1→4) bonds. Its outstanding properties, including biocompatibility, biodegradabillity and particular biological properties make this natural polymer an excellent candidate for biomedical and pharmaceutical uses (Ravi Kumar, 2000; Rinaudo, 2006). The research on Cs to produce nanomaterials intended for drug delivery systems started two decades ago looking for biocompatible alternatives to inorganic compounds, metals and synthetic polymer systems, which provided limited stability to transportation of proteins (Garcia-Fuentes & Alonso, 2012). Chitosan based nanomaterials are commonly produced inducing inter-chain crosslinking by covalent bonds or ionic interactions, but certainly there are diverse preparation processes that have been proposed to improve their functional properties, such as size, stability, surface charge or drug loading capacity (Calvo, Remuñán-López, Vila-Jato, & Alonso, 1997; Ohya, Shiratani, Kobayashi, & Ouchi, 1994).

Several applications based on chitosan nanoparticles carriers have been described, including vaccine, gene and drug delivery systems (Garcia-Fuentes & Alonso, 2012; Younes & Rinaudo, 2015). In most of these applications the Cs nanoparticles are in colloidal suspension. However, the use of dry nanoparticles could improve the stability and storage life of drug delivery systems. Furthermore, dry nanoparticles are usually preferred in certain applications, such as formulations for inhalation (Grenha, Seijo, & Remuñán-López, 2005). Chitosan dry materials have been proposed as controlled release devices based on their considerable specific surface area, porous structure properties and capacity to incorporate bioactive compounds, particularly protein drugs and enzymes (Ulker & Erkey, 2017). Generally evaporation (e.g. spray-drying) or sublimation (e.g. freeze-drying) procedures are used to obtain dry chitosan nanoparticles (Abdelwahed, Degobert, Stainmesse, & Fessi, 2006; Grenha et al., 2005; Ngan et al., 2014). The supercritical CO_2 ($scCO_2$)

drying is an alternative method that can produce dry porous materials from previously formed gels. The modifications of the structural features of the materials could be reduced to minimum due to the solvation capacity and low surface tension of the $scCO_2$ (Valentin, Molvinger, Quignard, & Brunel, 2003). Usually, the materials obtained by $scCO_2$ drying have larger specific surface areas, low density and highly porous structure, providing appealing properties for active transport of bioactive substances (Zarzycki, Modrzejewska, Dorabialska, Rogacki, & Wojtasz-Pająk, 2009). The production of Cs materials obtained by $scCO_2$ drying of chemical or physical gels as monoliths or microparticles has been reported previously (Ennajih, Bouhfid, Essassi, Bousmina, & El Kadib, 2012; Valentin, Bonelli, Garrone, Di Renzo, & Quignard, 2007). Recently, was reported the $scCO_2$ drying of chitosan ionotropic nanogels with aerogel characteristics (i.e. large surface area and porosity) in nano scale (Caro León et al., 2017). Based on the background, a $scCO_2$ dried gels formed by chitosan nanoparticles have structural properties and stability to provide a good loading and controlled release capacity for the βlg, allows its application in dry and aqueous media.

The aim of this study was investigate the properties of $scCO_2$ dried chitosan nanoparticles as bioactive compounds carrier. Dry chitosan nanoparticles loaded with a protein, β-lactoglobulin (βlg), were produced and the loading parameters calculated. The physicochemical characteristics of the loaded dry chitosan nanoparticles were reported. As β-lactoglobulin is one of the milk proteins showing antioxidant activity (Liu, Chen, & Mao, 2007; Mengíbar, Miralles, & Heras, 2017; Stanic-Vucinic, Prodic, Apostolovic, Nikolic, & Velickovic, 2013), it was determined in the loaded nanoparticles, along with the biocompatibility to cultured cells and the structural properties of the released protein, in order to estimate the functionality of the carrier.

2. Experimental

2.1 Materials

Chitosan (Cs) with degree of acetylation (DA) of 20% and weight average molecular weight (Mw) of 250 kDa was provided by Primex EHF (Iceland). β-Lactoglobulin (βlg) from bovine milk with Mw of 18.4 kDa and purity higher than 90% was obtained from Sigma-Aldrich (USA). Reagent grade solvents and chemicals, acquired from recognized commercial distributors, were used. Deionized water was utilized throughout unless otherwise stated.

2.2 Nanoparticle preparation

Chitosan nanoparticles (CsN) and dry chitosan nanoparticles (DCsN) were obtained according to previously reported procedures (Caro León et al., 2017; Goycoolea, Lollo, Remuñán-López, Quaglia, & Alonso, 2009). To obtain dry chitosan nanoparticles loaded with β-lactoglobulin

(DCsNβ) the following procedure modification were implemented. Briefly, 30 mL of 1 mg/mL Cs solution in 2% v/v CH_3COOH including the protein (1 mg/mL βlg) was mixed with 20 mL of 1.0 mg/mL sodium tripolyphosphate (TPP) solution. The subsequent drying of the obtained Cs nanoparticles including βlg (CsNβ) with $scCO_2$ was performed as described previously (Caro León et al., 2017).

2.3 Physicochemical characterization

The association efficiency (AE) and loading efficiency (LE) of βlg in the CsNβ was calculated the following equations (1 and 2, respectively):

$$AE = [(P_0 - P_s)/P_0] \times 100 \quad (1)$$

$$LE = [(P_0 - P_s)/N] \times 100 \quad (2)$$

where P_0 is the initial amount of protein (βlg) added to the system; P_S is the quantity of βlg not included in the nanoparticles, it was measured by UV-Vis spectrophotometry (λ=280 nm) in the supernatant of centrifuged nanoparticles (24000g, 45 min at 25°C); and N is the dry weight of the nanoparticles. All the measurements were obtained by triplicate.

The hydrodynamic diameter and zeta (ζ) potential of the nanoparticles in colloidal suspension was determined by dynamic light scattering with a non-invasive back scattering (DLS/NIBS) technology and laser Doppler electrophoresis with phase analysis light scattering (M3-PALS) using a Zetasizer Nano-ZS (ZEN 3600, Malvern instruments, UK). The morphology of the nanoparticles was studied by field emission-scanning electron microscopy (FE-SEM) using a SU 8000 Hitachi microscopy. To this end, 10 μL of nanoparticles suspension was dropped on a copper grid coated with a Formvar membrane, allowed to stand for 5 minutes, dried, and coated with Au/Pd.

Several techniques used to determine the main characteristics of the dry nanoparticles. Solid-state cross-polarization magic angle spinning ^{13}C nuclear magnetic resonance (CP/MAS-NMR) was performed in a Bruker Avance TM 400WB equipped with a wide-mouth superconducting magnet (89 mm) operating at 9.4 Tesla. The experimental conditions were: 4.4 μs width 90° pulse with 4 s repetition time, 1 ms cross-polarization contact time and spectrum accumulation of 2000 scans. The samples were contained in a cylindrical ceramic rotor. Attenuated total reflection Fourier transform infrared (ATR-FTIR) spectra were collected on a Perkin-Elmer Spectrum One spectrophotometer; using 64 co-added scans with 4 cm^{-1} resolution over a spectrum range of 400-6000 cm^{-1}. Thermogravimetric measurements (TGA) was performed on a Q500 thermogravimetric analyzer (TA instruments), heating from 20° up to 800°C at 10°C/min, under nitrogen flow. X-ray diffraction (XRD) experiments were carried out on a Bruker D8 Advance diffractometer equipped with CuKα radiation. The angle range (2θ) was scanned from 2° to 40° at a step size of 0.02°. The working voltage and current were 45 kV and 100 mA, respectively. The crystallinity index (CrI) was calculated from the corresponding XRD diffractogram using the following equation (3):

$$\mathrm{CrI}\ (\%) = [(I_{110} - I_{am})/I_{110}] \times 100 \qquad (3)$$

where I_{110} is the maximum intensity of the 110 plane at 2θ=20°, and I_{am} is the intensity of the amorphous diffraction at 2θ=16° (Vishu Kumar, Varadaraj, Lalitha, & Tharanathan, 2004).

Specific surface area of the dry nanoparticles was determined by means of nitrogen sorption on a Monosorb Surface Area Analyser MS-13 (Quantachrome). With this purpose the samples were degassed at 80°C for 18 hours under vacuum prior to analysis. Six points in the range of relative pressure (P/P_0) from 0.05 to 0.3 were used to calculate the surface area by Brunauer–Emmett–Teller (BET) method.

To determine the effect of the $scCO_2$ drying on the loading capacity of the nanoparticles, a sample of DCsNβ was resuspended (0.5 mg/mL) in 2% v/v CH_3COOH (pH 3.1) under constant vigorous magnetic stirring during 24 hours and then filtered through a 0.22 μm pore filter. The protein content in the supernatant and in the resuspended nanoparticles was determined by UV-Vis spectrophotometry at λ of 280 nm. The AE and LE parameters were calculated using equations (1) and (2). The hydrodynamic size, ζ-potential and morphological observation of the resuspended samples were also characterized as described before.

Protein release studies were performed by incubating 15 mg of DCsNβ in 5 mL of either pH 7.4 acetate buffer or 2% v/v CH_3COOH solution (pH 3.1), in 25°C bath with continuous stirring. Aliquots of 1 mL were taken at time intervals (3, 6, 9, 12, 24, 27 30, 33 and 48 hours), replacing the volume with the corresponding media. The nanoparticles were removed from the aliquots by filtration through 0.22 μm pore size nylon membranes (Millipore), then the amount of βlg released was determined by UV-Vis spectroscopy at λ of 280 nm using calibration curves at the respective pH value.

Circular dichroism (CD) was used to determine the possible effects of immovilization and $scCO_2$ drying on the protein secondary structure conformation. The analysis was performed on protein released from DCsNβ on a J-815 spectropolarimeter (Jasco) using a 1 mm path length quartz cell at 25°C. All the spectra were recorded in the 200-240 nm range. A βlg solution in 2% v/v CH_3COOH (pH 3.1) was used as reference. The relative proportion of secondary conformation structures was calculated using the Dichroweb tools (http://dichroweb.cryst.bbk.ac.uk) available in the World Wide Web (Whitmore & Wallace, 2008).

2.4 Evaluation of antioxidant activity

The antioxidant activity of the DCsNβ was estimated by the 2,2-diphenyl-1-picrylhydrazy (DPPH) free radical scavenging method. Briefly, 1.0 mL of ethanolic DPPH solution (0.127×10^{-3} M) was mixed with the same volume of resuspended DCsNβ particles (0.5 mg/mL). The absorbance variation at 515 nm was monitored every 30 min using a Biotek Synergy HT detector. The radical scavenging activity (RSA) was calculated using Equation (4):

$$RSA(\%) = [(A_0 - A_1)/A_0] \times 100 \qquad (4)$$

where A_0 and A_1 correspond to the absorbance at 515 nm of the mixture in the absence or presence of antioxidant, respectively.

3. Results and discussion

3.1 Preparation and characterization of nanoparticles

Under the used conditions was possible to reproduce the production of chitosan nanoparticles including βlg. The CsNβ produced by ionotropic gelation have spherical shape as appear in the FE-SEM image (Figure 1). Size measurements of individual particles were in the range of 87 to 295 nm. This is consistent with results found in literature for similar chitosan nanoparticles (Calvo et al., 1997). According to the DLS measurements, the average hydrodynamic diameter of the CsNβ was 90 nm (PDI = 0.26) with a ζ-potential of +17 ±4 mV. Previously reported chitosan nanoparticles (CsN) have similar size (Caro León et al., 2017). Apparently, the presence of βlg, at the used quantity, do not affect largely the size of the nanoparticles when are produced by the same procedure and Cs characteristics. Conversely, there is a difference of ζ-potential, nanoparticles without protein have reach higher positive value (+27 ±4 mV). The difference arise from the anionic nature of βlg in neutral and acidic pH over its isoelectric point (5.2) (Chen & Subirade, 2005); in such conditions ionic interactions among chitosan and βlg or molecular re-arrangements at the surface of the particle could be responsible of the reduction of the net surface charge of the nanoparticles.

Figure 1. FE-SEM image of the CsNβ, Magnification of 30,000X, SE detector, 1.5 kV.

The protein loading parameters are useful to evaluate the suitability of the nanoparticle production process to incorporate βlg. In one hand, the association efficiency (AE) indicates the proportion the initial protein is effectively incorporated in the nanoparticles. The AE of the CsNβ was 74.2%. On

the other hand, the loading efficiency (LE) is the mass proportion of protein in the produced material. For CsNβ the LE was 37.1%. The loading parameters of the CsNβ production reach high marks compared with similar chitosan nanoparticles production reports (Chen & Subirade, 2005). The obtained values were used as benchmarks to determine how affect the $scCO_2$ drying on the final material. Apparently the $scCO_2$ drying do not caused significant loss of the incorporated protein since the DCsNβ have 70.1% of AE and 33.0% of LE. Several types of interactions (e.g. electrostatic, hydrophobic, hydrogen bonding) can occur between chitosan and βlg molecules leading to complexation that could be stable at different conditions (Ha, Kim, Lee, & Lee, 2013). Accordingly, it can be argued that the solvents and conditions used in the $scCO_2$ drying process do not promote the release of the βlg loaded in the chitosan nanoparticles.

Several analytical techniques were used in order to shed light on the influence of the presence of the βlg and $scCO_2$ drying process on the structure of the DCsNβ. The specific surface area was measured by N_2 sorption method using the BET model. The DCsNβ has a specific surface area of 12.10 m^2/g, while DCsN has 10.76 m^2/g. The N_2 adsorption isotherms of the dry nanoparticles resemble the IUPAC classification type IV isotherm with hysteresis loop (Figure S1, supplementary material). This behavior has been associated with capillary condensation into mesopores and the limiting uptake over a range of high relative pressure (Sing, 2009). The effects of the $scCO_2$ drying over the gel network structure of the nanoparticles have been associated mainly to the required successive replacement of liquid phase, each with different solvation interaction with the chitosan (Caro León et al., 2017). However the polymeric network structure disturbance is considerably lower than in drying procedures based on solvent evaporation or sublimation. Accordingly, $scCO_2$ drying of polysaccharide gels normally produce mesoporous and extended specific surface area materials (García-González, Alnaief, & Smirnova, 2011). The DCsNβ and DCsN are slightly different surface area; this could be related to the presence of βlg.

The CP/MAS ^{13}C-NMR spectra of Cs, βlg and DCsNβ are shown in Figure 2. The Cs spectrum display bands at 57.6, 60.9, 76.1, 84 and 105.7 ppm that correspond to the carbon atoms of the pyranose rings (C2, C6, C5+C3, C4, C1; respectively); the bands at 23 and 178 ppm are associated to the methyl and carbonyl carbons of the acetyl group of the N-acetyl-glucosamine units, respectively (Saito, Tabeta, & Ogawa, 1987). For The βlg, the peak at 173.9 ppm is attributed to backbone carbonyls and the peaks at about 53.8 ppm corresponding to backbone α-CH carbons. Also, the three other peaks between at 25.4, 40.2 and 301.1 ppm are attributed to aliphatic side-chain carbons (Assifaoui et al., 2014; Fernandez, Reimer, & Denn, 1992). Has would be expected, the DCsNβ spectrum display features of both, Cs and βlg. It shows peaks corresponding to Cs C1 and C3+C5 with lower resolution. This has been related to anisotropic effects of amorphous structures in the $scCO_2$ dried Cs nanoparticles (Caro León et al., 2017). Also, the DCsNβ spectrum show protein related peaks practically the same position, except for the one at 53.8 ppm that is shifted to 58.3 ppm, presumably due conformational changes in the incorporated protein. The observed bands in the DCsNβ spectrum confirmed the presence of the protein in the material.

The ATR-FTIR spectra of Cs, βlg and DCsNβ are included in Figure 3. For Cs, the main bands observed are centered at 3355, 2875, 1650, 1584, 1417, 1375, 1316 cm^{-1} and several overlapped bands in the fingerprint region (1200-850 cm^{-1}). This coincides with the reference infrared absorption pattern for Cs. For the βlg, The bands at 1623 cm^{-1} and 1545 cm^{-1} are attributed to amide

I (C=O bond stretching) and amide II (C—N bond stretching coupled with N—H bending mode), respectively (Brugnerotto et al., 2001). Several changes are observed in the DCsNβ spectrum: the bands corresponding to the O-H and N-H stretching vibrations (3350 and 2875 cm^{-1}, respectively) becomes broader, that indicates such bonds are involved in a larger variety of chemical environments including multiple hydrogen bonding induced by the ionic crosslinking between Cs and TPP. The band at 1632 cm^{-1} is also broader which suggest an increasing of intermolecular interactions in the material (Takeshita & Yoda, 2015).The C=O and NH_2 vibrations bands (1650 and 1584 cm^{-1}, respectively) are shifted to lower wavenumbers. The bands at 1218 cm^{-1} and 892 cm^{-1} in the DCsNβ spectrum are attributed to P=O stretching vibration and P-O-P asymmetric stretching vibration, which also appear in the TPP spectrum (Walke et al., 2015). The bands corresponding amide I and amide II of βlg spectrum appear strongly in the DCsNβ at the same wavelength that indicates the presence of protein in the material.

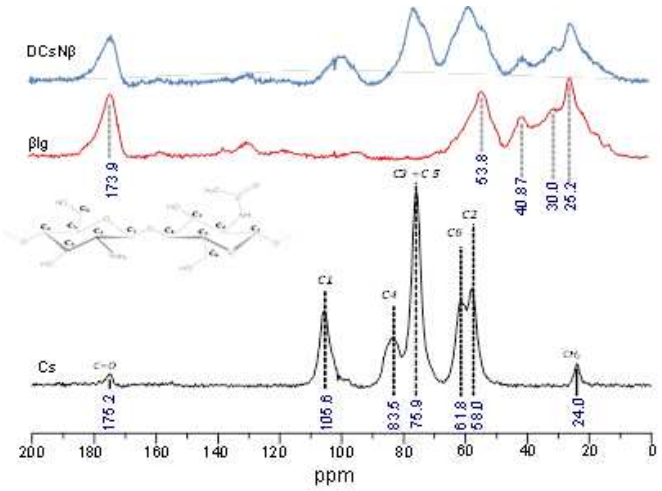

Figure 2. CP/MAS ^{13}C-NMR spectra of Cs (—), βlg (—) and DCsNβ (—).

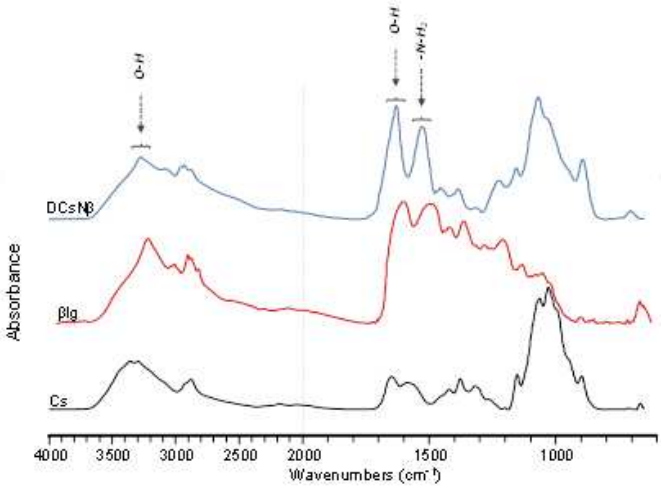

Figure 3. ATR-FTIR spectra of Cs (—), βlg (—) and DCsNβ (—)

To determine the thermal stability of the materials, thermogravimetric (TG) and differential thermogravimetric (DTG) curves of Cs, βlg and DCsNβ were obtained (Figure 4). Three main steps are observed in the thermogram of Cs; the first one goes up to 130°C and is attributed to the moisture evaporation and cause 7% of mass loss. The second step corresponds to the main degradation of the polyssacharide, with 40% of weight loss associated and highest rate close to 300°C. This phase involves the dehydration of the saccharide rings, thermal depolymerization and decomposition of the Cs units (Fernández-Quiroz et al., 2015; Peniche et al., 2007; Walke et al., 2015). The last step, related to secondary thermolysis processes, occurs over 400°C leaving less than 10% of residual mass. The TG curve of the βlg shows a first step of water loss similar to the Cs curve. Also, a broad mass loss (around 48%) occurred around 320°C and it is attributed to the polypeptide chain thermal decomposition of proteins (Duce et al., 2017). In addition, it has been reported that TG curves of βlg in O_2 atmosphere decomposes into two steps at about 490°C (76%) and 580°C (96%). The capacity of the βlg to form dimers, oligomers and aggregated species has been described previously and the losses at 490°C (βlg) can be related to the decomposition of aggregated portions of proteins, while the sharp mass loss above 550°C is related to the carbonizing and ashing of the hard residues of the proteins (Duce et al., 2017).

The first weight loss stage of DCsNβ is shorter than in Cs, which is attributed to less dense structure. Furthermore, the thermal degradation of DCsNβ starts at lower temperature than in Cs. The stability of the untreated chitosan could be related with the presence of higher amount of microcrystalline domains that give relative stability at elevated temperature. The char yield (residual mass after pyrolysis) for Cs and DCsNβ was 6 and 38% at 800°C, respectively. Apparently the presence of TPP (inorganic matter) affects the outcome of the thermal reactions. In general, the processes involved to produce DCsNβ cause the start of disintegration at lower temperatures that could be associated with higher relative rigidity of the internal structure in DCsNβ, due to multiple intermolecular interactions between the polymer and the protein.

The DTG of the Cs shown a maximum at 295°C which corresponds to the beginning of the degradation of the polymer. For the βlg it has been reported three main peaks around 300°C, 490°C and 583°C (Duce et al., 2017). In our study the DTG of βlg has two main peaks at 300 and 550°C. These differences could be attributed due that the reported study was in an O_2 atmosphere while our experiments were performed at N_2 that could reduce the pyrolysis effect. The DTG of DCsNβ has a maximum at 308°C similar to the βlg, however, the peak a 550°C did not appear and it has a new peak at 240°C. This could be associated to reduction in the thermal stability of the DCsNβ due the specific interaction product between the Cs and the protein and also due the crosslinking of the polymer.

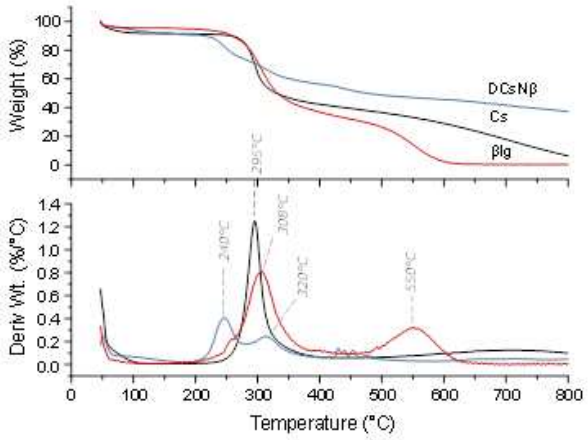

Figure 4. TGA and DTG curves of Cs (—), βlg (—) and DCsNβ (—).

XRD analysis was perfomed to determine the crystallinity of the DCsNβ (Figure S2). Cs shows diffraction peaks at 2θ = 9.8° and 20° corresponding to the equatorial (020) and (110) of the microcrystalline reflections of the polyssacharide (Sakurai, Shibano, Kimura, & Takahashi, 1985; Zhang, Xue, Xue, Gao, & Zhang, 2005). The main diffractive regions of the βlg were centered at 8° and 19°. For DCsNβ the signal have its higher values centred at 9° and 18° with notoriously lower intensity. The crystallinity index for Cs and DCsNβ was 59.5% and 33.2% respectively. This indicates the lower quantity ordered molecular structures in the βlg loaded nanoparticles. Similar results were reported for Cs gels dried with $scCO_2$ treatment (Takeshita & Yoda, 2015).

To explore the behaviour of the DCsNβ in aqueous suspension and evaluate the possible applications of this material, resuspension test in diluted acid (CH_3COOH 2% v/v, pH 3.1) and pure water were performed. When DCsNβ are stirred into acidic medium the particles were solvated and an opalescent suspension was obtained. However, the ionic crosslinks stands against the acid conditions (pH ~4) hindering the dissolution process of the Cs. As can be observed in the FE-SEM image (Figure 5) apparently the resuspended particles are formed by aggregated individual nanoparticles with spherical shape. A different outcome was observed in pure water where considerable portion of the material remains as visible particles at the bottom of the vessel. According to DLS measurements, the size of the resuspended DCsNβ in diluted acid was 333 nm (PDI= 0.43) and the ζ potential reaches a value of +56 ±5 mV. The increase of ζ potential compared with the CsNβ may be related with molecular re-arrangements induced by the protonation of available amino groups of polysaccharide chains in acidic environment. In such conditions, is expected that DCsNβ form stable colloidal suspensions; ζ potential values above +50 mV are associated to systems with good stability (Bhattacharjee, 2016).

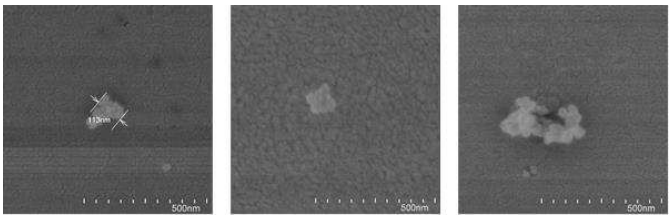

Figure 5. FE-SEM image of a resuspended DCsNβ particle. Magnification of 150,000X; SE detector, 1.5 kV.

According to the literature, the formation of βlg-Cs complexes is drive mainly by electrostatic interactions (Guzey & McClements, 2006; A.-C. Lee & Hong, 2009; P. S. Lee, Yim, Choi, Van Anh Ha, & Ko, 2012). Since the net ionic charge of βlg goes from negative to positive as the pH decrease, the effect of the pH on the release of βlg from DCsNβ was investigated. The Figure 6 shows the release profile of the protein from the polymeric matrix. At pH 7.4, the release of the protein is practically inexistent that could be attributed to the strong electrostatic interaction between both components. Conversely, at pH 3.1 a burst like release is observed; up to 40% of the protein is found in the suspension medium within the first 10 hours. However, although the pH is not favorable for electrostatic interaction between βlg and Cs, most of the protein (~58%) remains associated with the DCsNβ at the end of the experiment (50 h). Several factors could play a role in the observed behavior. For example, the presence of non-electrostatic interactions (e.g. hydrophobic, H-bonds) stabilizing the formed βlg-Cs complexes, the lower solubility of βlg at such pH and ionic strength or the formation of βlg aggregates that cannot leave the network structure of the nanoparticles (Mounsey, O'Kennedy, Fenelon, & Brodkorb, 2008).

Circular dichroism is a useful spectroscopic technique to describe the secondary conformation of proteins in terms of β-sheets, α-helical, β-strand and unordered structures content. The CD spectra of βlg before incorporation and after released from DCsNβ shown minimum value around 233 and 230 nm, respectively (Figure S3). The observed spectra type has been related to β-sheet structures (Zheng, Liu, Zhu, Zheng, & Liu, 2016). The proportion of secondary conformation structures of the βlg was 13.9% α-helix, 35.5% β-sheet, 28.3% β-turn and 22.3% unordered structures while for the DCsNβ released βlg was 10.1% α-helix, 30.3% β-sheet, 24.5% β-turn and 35.1% for unordered structures. The reduction of ordered structures in the released protein could be result of the multiple interactions with the Cs matrix and possible mild denaturation induced through the solvent exchange of the drying process (Uversky, Narizhneva, Kirschstein, Winter, & Löber, 1997).

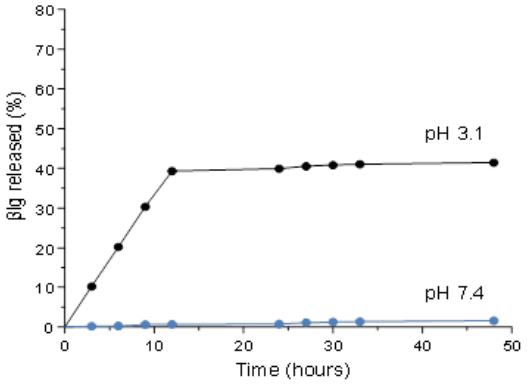

Figure 6. Release profile of the βlg from DCsNβ at pH 3.1 (—) and 7.4 (—).

3.2 Evaluation of antioxidant activity

The antioxidant activity of the resuspended DCsNβ and native βlg solution were analyzed by the DPPH assay and the results are shown in the Figure 7. The study determines the reduction of active DPPH free radicals by the reaction with the antioxidant compound. The native βlg solution has an appreciable antioxidant activity confirming previous reports that increase with the time and corresponds to 47% at 24 hours (Liu et al., 2007; Stanic-Vucinic et al., 2013). The resuspended DCsNβ has less antioxidant activity compared with the native protein; however, it reached 31% at 24 hours of reaction. The βlg is a milk protein that possesses antioxidant activity; however, its contribution to total activity relative to the other milk proteins has not been completely established. Using anti-lactoglobulin antibodies, it has been observed that βlg contributes approximately 50% of the total activity. The exact antioxidant mechanism of the protein is remaining unknown, but some has been proposed. For example, it has been estimated that the free radical scavenging is obtained by the chelation between the amino acids residues and pro-oxidative transition metals (Liu et al., 2007; Stanic-Vucinic et al., 2013). Other studies indicated that the Cys-121 of βlg is directly related with the antioxidant effect due to its sulfhydryl groups capable of donating hydrogen (Allen & Wrieden, 1982; Elias, McClements, & Decker, 2005). As we could demonstrate in the βlg release section, around of 50 % of the protein remains linked to the DCsNβ due the strong electrostatic interaction between Cs and βlg. In the other hand, it was reported that Cs and its derivatives act as antioxidants by scavenging oxygen radicals such as hydroxyl, superoxide, alkyl as well as highly stable DPPH radicals tested in vitro. The mechanism of radical scavenging activity of Cs is attributed to reaction between hydroxyl and amino groups (attached to C-2, C-3 and C-6 of the pyranose ring) with unstable free radicals to produce stable macromolecule radicals (Younes & Rinaudo, 2015). The results showed that the antioxidant capacity of the DCsNβ could be attributed to the synergic activity of the protein and the polysaccharide and its reduction (compared with the protein solution) could be related with the availability of specific groups in the Cs or βlg due the crosslinking and the solvent change. The results indicate that our materials could be used as an interesting antioxidant device; however, more studies are needed to elucidate the antioxidant mechanism.

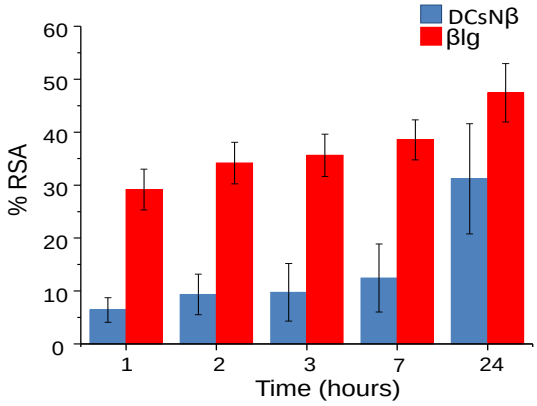

Figure 7. Experimental radical scavenging activity (RSA) of DPPH in presence of βlg isolated from the DCsNβ and native βlg solution. Data represent mean ± S.D. (n = 5).

4. Conclusions

In this work, dried gels based on chitosan nanoparticles incorporating β-lactoglobulin were produced using ionotropic gelation and supercritical CO_2 drying methods. Spherical nanoparticles were produced with hydrodynamic diameter of about 100 nm with positive surface charge in aqueous suspension. The supercritical CO_2 drying process generates materials that appear the accumulation of the individual nanoparticles but retaining interesting structural properties related to aerogels, extended surface area and high porosity. The obtained DCsNβ probe the possibility to incorporate protein in $scCO_2$ dried chitosan nanoparticles. The physicochemical and thermal characterization demonstrates the stability of these materials. The DCsNβ have high protein loading parameters can be resuspended in acidic media with partial release of the βlg. The antioxidant and biocompatibility properties of the resuspended DCsNβ suggest the possibility to apply them as a nutraceutical and biomedical applications. Furthermore, the applied method could lead to produce innovative carrier devices based on polysaccharides and other biopolymers.

Acknowledgements

The authors want acknowledge the financial support of CONACYT through the Project CB-2011-01-169626 and the fellowship DC2013-256 for JCL. Similarly, it is highly appreciated the valuable input of the Biomaterials Group of the ICTP-CSIC and the technical staff of the Biopolymer Research Group of CIAD.

References

Abdelwahed, W., Degobert, G., Stainmesse, S., & Fessi, H. (2006). Freeze-drying of nanoparticles: Formulation, process and storage considerations. Advanced Drug Delivery Reviews, 58(15), 1688–1713.

Allen, J. C., & Wrieden, W. L. (1982). Influence of milk proteins on lipid oxidation in aqueous emulsion: I. Casein, whey protein and α-lactalbumin. Journal of Dairy Research, 49(2), 239–248.

Assifaoui, A., Huault, L., Maissiat, C., Roullier-Gall, C., Jeandet, P., Hirschinger, J., … Loupiac, C. (2014). Structural studies of adsorbed protein (betalactoglobulin) on natural clay (montmorillonite). RSC Advances, 4(105), 61096–61103.

Bhattacharjee, S. (2016). DLS and zeta potential – What they are and what they are not? Journal of Controlled Release, 235, 337–351.

Brugnerotto, J., Lizardi, J., Goycoolea, F. M., Argüelles-Monal, W., Desbrieres, J., & Rinaudo, M. (2001). An infrared investigation in relation with chitin and chitosan characterization. Polymer, 42(8), 3569–3580.

Calvo, P., Remuñán-López, C., Vila-Jato, J. L., & Alonso, M. J. (1997). Novel hydrophilic chitosan-polyethylene oxide nanoparticles as protein carriers. Journal of Applied Polymer Science, 63(1), 125–132.

Caro León, F. J., Lizardi-Mendoza, J., Argüelles-Monal, W., Carvajal-Millan, E., Franco, Y. L. L., & Goycoolea, F. M. (2017). Supercritical CO2 dried chitosan nanoparticles: production and characterization. RSC Advances, 7(49), 30879–30885.

Carvalho, E. L. S., Grenha, A., Remuñán-López, C., Alonso, M. J., & Seijo, B. (2009). Mucosal delivery of liposome-chitosan nanoparticle complexes. Methods in Enzymology, 465, 289–312.

Cavalli, R., Leone, F., Minelli, R., Fantozzi, R., & Dianzani, C. (2014). New Chitosan Nanospheres for the Delivery of 5-Fluorouracil: Preparation, Characterization and in vitro Studies. Current Drug Delivery, 11(2), 270–278.

Chen, L., & Subirade, M. (2005). Chitosan/beta-lactoglobulin core-shell nanoparticles as nutraceutical carriers. Biomaterials, 26(30), 6041–6053.

Duce, C., Porta, V. D., Bramanti, E., Campanella, B., Spepi, A., & Tiné, M. R. (2017). Loading of halloysite nanotubes with BSA, α -Lac and β -Lg: a Fourier transform infrared spectroscopic and thermogravimetric study. Nanotechnology, 28(5), 055706.

Elias, R. J., McClements, D. J., & Decker, E. A. (2005). Antioxidant activity of cysteine, tryptophan, and methionine residues in continuous phase beta-lactoglobulin in oil-in-water emulsions. Journal of Agricultural and Food Chemistry, 53(26), 10248–10253.

Ennajih, H., Bouhfid, R., Essassi, E. M., Bousmina, M., & El Kadib, A. (2012). Chitosan–montmorillonite bio-based aerogel hybrid microspheres. Microporous and Mesoporous Materials, 152, 208–213.

Fakruddin, M., Hossain, Z., & Afroz, H. (2012). Prospects and applications of nanobiotechnology: a medical perspective. Journal of Nanobiotechnology, 10, 31.

Fernandez, V. L., Reimer, J. A., & Denn, M. M. (1992). Magnetic resonance studies of polypeptides adsorbed on silica and hydroxyapatite surfaces. Journal of the American Chemical Society, 114(24), 9634–9642.

Fernández-Gutiérrez, M., Bossio, O., Gómez-Mascaraque, L. G., Vázquez-Lasa, B., & San Román, J. (2015). Bioactive Chitosan Nanoparticles Loaded with Retinyl Palmitate: A Simple Route Using Ionotropic Gelation. Macromolecular Chemistry and Physics, 216(12), 1321–1332.

Fernández-Quiroz, D., González-Gómez, Á., Lizardi-Mendoza, J., Vázquez-Lasa, B., Goycoolea, F. M., San Román, J., & Argüelles-Monal, W. M. (2015). Effect of the molecular architecture on the thermosensitive properties of chitosan-g-poly(N-vinylcaprolactam). Carbohydrate Polymers, 134, 92–101.

Garcia-Fuentes, M., & Alonso, M. J. (2012). Chitosan-based drug nanocarriers: where do we stand? Journal of Controlled Release: Official Journal of the Controlled Release Society, 161(2), 496–504.

García-González, C. A., Alnaief, M., & Smirnova, I. (2011). Polysaccharide-based aerogels—Promising biodegradable carriers for drug delivery systems. Carbohydrate Polymers, 86(4), 1425–1438.

Goimil, L., Braga, M. E. M., Dias, A. M. A., Gómez-Amoza, J. L., Concheiro, A., Alvarez-Lorenzo, C., … García-González, C. A. (2017). Supercritical processing of starch aerogels and aerogel-loaded poly(ε-caprolactone) scaffolds for sustained release of ketoprofen for bone regeneration. Journal of CO2 Utilization, 18, 237–249.

Goycoolea, F. M., Lollo, G., Remuñán-López, C., Quaglia, F., & Alonso, M. J. (2009). Chitosan-Alginate Blended Nanoparticles as Carriers for the Transmucosal Delivery of Macromolecules. Biomacromolecules, 10(7), 1736–1743.

Grenha, A., Seijo, B., & Remuñán-López, C. (2005). Microencapsulated chitosan nanoparticles for lung protein delivery. European Journal of Pharmaceutical Sciences, 25(4–5), 427–437.

Guzey, D., & McClements, D. J. (2006). Characterization of β-lactoglobulin–chitosan interactions in aqueous solutions: A calorimetry, light scattering, electrophoretic mobility and solubility study. Food Hydrocolloids, 20(1), 124–131.

Ha, H.-K., Kim, J. W., Lee, M.-R., & Lee, W.-J. (2013). Formation and characterization of quercetin-loaded chitosan oligosaccharide/β-lactoglobulin nanoparticle. Food Research International, 52(1), 82–90.

Larson, N., & Ghandehari, H. (2012). Polymeric Conjugates for Drug Delivery. Chemistry of Materials, 24(5), 840–853.

Lee, A.-C., & Hong, Y.-H. (2009). Coacervate formation of α-lactalbumin–chitosan and β-lactoglobulin–chitosan complexes. Food Research International, 42(5–6), 733–738.

Lee, P. S., Yim, S. G., Choi, Y., Van Anh Ha, T., & Ko, S. (2012). Physiochemical properties and prolonged release behaviours of chitosan-denatured β-lactoglobulin microcapsules for potential food applications. Food Chemistry, 134(2), 992–998.

Liu, H. C., Chen, W. L., & Mao, S. J. T. (2007). Antioxidant nature of bovine milk beta-lactoglobulin. Journal of Dairy Science, 90(2), 547–555.

Mengíbar, M., Miralles, B., & Heras, Á. (2017). Use of soluble chitosans in Maillard reaction products with β-lactoglobulin. Emulsifying and antioxidant properties. LWT - Food Science and Technology, 75, 440–446.

Mohanraj, V. J., Barnes, T. J., & Prestidge, C. A. (2010). Silica nanoparticle coated liposomes: A new type of hybrid nanocapsule for proteins. International Journal of Pharmaceutics, 392(1–2), 285–293.

Mounsey, J. S., O'Kennedy, B. T., Fenelon, M. A., & Brodkorb, A. (2008). The effect of heating on β-lactoglobulin–chitosan mixtures as influenced by pH and ionic strength. Food Hydrocolloids, 22(1), 65–73.

Ngan, L. T. K., Wang, S.-L., Hiep, Đ. M., Luong, P. M., Vui, N. T., Đinh, T. M., & Dzung, N. A. (2014). Preparation of chitosan nanoparticles by spray drying, and their antibacterial activity. Research on Chemical Intermediates, 40(6), 2165–2175.

Ohya, Y., Shiratani, M., Kobayashi, H., & Ouchi, T. (1994). Release Behavior of 5-Fluorouracil from Chitosan-Gel Nanospheres Immobilizing 5-Fluorouracil Coated with Polysaccharides and Their Cell Specific Cytotoxicity. Journal of Macromolecular Science, Part A, 31(5), 629–642.

Peniche, C., Fernández, M., Rodríguez, G., Parra, J., Jimenez, J., Bravo, A., … San Román, J. (2007). Cell supports of chitosan/hyaluronic acid and chondroitin sulphate systems. Morphology and biological behaviour. Journal of Materials Science: Materials in Medicine, 18(9), 1719–1726.

Ravi Kumar, M. N. . (2000). A review of chitin and chitosan applications. Reactive and Functional Polymers, 46(1), 1–27.

Rinaudo, M. (2006). Chitin and chitosan: Properties and applications. Progress in Polymer Science, 31(7), 603–632.

Safari, J., & Zarnegar, Z. (2014). Advanced drug delivery systems: Nanotechnology of health design A review. Journal of Saudi Chemical Society, 18(2), 85–99.

Saito, H., Tabeta, R., & Ogawa, K. (1987). High-resolution solid-state carbon-13 NMR study of chitosan and its salts with acids: conformational characterization of polymorphs and helical structures as viewed from the conformation-dependent carbon-13 chemical shifts. Macromolecules, 20(10), 2424–2430.

Sakurai, K., Shibano, T., Kimura, K., & Takahashi, T. (1985). Crystal Structure of Chitosan. *Sen'i* Gakkaishi, 41(9), T361–T368.

Sing, K. S. W. (2009). Reporting physisorption data for gas/solid systems with special reference to the determination of surface area and porosity (Recommendations 1984). Pure and Applied Chemistry, 57(4), 603–619.

Stanic-Vucinic, D., Prodic, I., Apostolovic, D., Nikolic, M., & Velickovic, T. C. (2013). Structure and antioxidant activity of β-lactoglobulin-glycoconjugates obtained by high-intensity-ultrasound-induced Maillard reaction in aqueous model systems under neutral conditions. Food Chemistry, 138(1), 590–599.

Takeshita, S., & Yoda, S. (2015). Chitosan Aerogels: Transparent, Flexible Thermal Insulators. Chemistry of Materials, 27(22), 7569–7572.

Technical Committee: ISO/TC 194 Biological and clinical evaluation of medical devices. ISO10993–5. Tests for In Vitro Cytotoxicity, Pub. L. No. ISO10993–5, 5 Biological Evaluation of Medical Devices 34 (2009).

Ulker, Z., & Erkey, C. (2017). An advantageous technique to load drugs into aerogels: Gas antisolvent crystallization inside the pores. The Journal of Supercritical Fluids, 120, Part 2, 310–319.

Uversky, V. N., Narizhneva, N. V., Kirschstein, S. O., Winter, S., & Löber, G. (1997). Conformational transitions provoked by organic solvents in β-lactoglobulin: can a molten globule like intermediate be induced by the decrease in dielectric constant? Folding and Design, 2(3), 163–172.

Valentin, R., Bonelli, B., Garrone, E., Di Renzo, F., & Quignard, F. (2007). Accessibility of the Functional Groups of Chitosan Aerogel Probed by FT-IR-Monitored Deuteration. Biomacromolecules, 8(11), 3646–3650.

Valentin, R., Molvinger, K., Quignard, F., & Brunel, D. (2003). Supercritical CO2 dried chitosan: an efficient intrinsic heterogeneous catalyst in fine chemistry. New Journal of Chemistry, 27(12), 1690–1692.

Vishu Kumar, A. B., Varadaraj, M. C., Lalitha, R. G., & Tharanathan, R. N. (2004). Low molecular weight chitosans: preparation with the aid of papain and characterization. Biochimica et Biophysica Acta (BBA) - General Subjects, 1670(2), 137–146.

Walke, S., Srivastava, G., Nikalje, M., Doshi, J., Kumar, R., Ravetkar, S., & Doshi, P. (2015). Fabrication of chitosan microspheres using vanillin/TPP dual crosslinkers for protein antigens encapsulation. Carbohydrate Polymers, 128, 188–198.

Whitmore, L., & Wallace, B. A. (2008). Protein secondary structure analyses from circular dichroism spectroscopy: Methods and reference databases. Biopolymers, 89(5), 392–400.

Yang, K. W., Li, X. R., Yang, Z. L., Li, P. Z., Wang, F., & Liu, Y. (2009). Novel polyion complex micelles for liver-targeted delivery of diammonium glycyrrhizinate: In vitro and in vivo characterization. Journal of Biomedical Materials Research Part A, 88A(1), 140–148.

Younes, I., & Rinaudo, M. (2015). Chitin and Chitosan Preparation from Marine Sources. Structure, Properties and Applications. Marine Drugs, 13(3), 1133–1174.

Zarzycki, R., Modrzejewska, Z., Dorabialska, M., Rogacki, G., & Wojtasz-Pająk, A. (2009). Properties of Chitosan Microgranules Formed by Supercritical Fluid Processing. Drying Technology,

27(12), 1370–1378.

Zhang, Y., Xue, C., Xue, Y., Gao, R., & Zhang, X. (2005). Determination of the degree of deacetylation of chitin and chitosan by X-ray powder diffraction. Carbohydrate Research, 340(11), 1914–1917.

Zheng, G., Liu, H., Zhu, Z., Zheng, J., & Liu, A. (2016). Selenium modification of β-lactoglobulin (β-Lg) and its biological activity. Food Chemistry, 204, 246–251.